Pore Size Heterogeneity and the Carbon Slit Pore: A Density Functional Theory Model

Christian Lastoskie,[*,†] Keith E. Gubbins,[†] and Nicholas Quirke[†,‡]

School of Chemical Engineering, Cornell University, Ithaca, New York 14853, and BP Research Centre, Middlesex TW16 7LN, U.K.

We present model isotherms predicted by nonlocal density functional theory for adsorption of simple fluids in carbon slit pores. The effects of pore size, temperature, and solid–fluid potential interaction strength are examined. Our results are summarized into a classification scheme based upon regimes of continuous pore filling, capillary condensation, and $0 \rightarrow 1$ layering transitions. The descriptions we have devised depart from the IUPAC convention in that the filling behavior, rather than the physical width of the pore, is used as a guide to classification. Our results suggest that while the magnitude of the solid–fluid interactions dictates the pressure at which pore filling occurs, the type of filling depends primarily upon the ratio of pore width to adsorbate molecular diameter. The critical pore widths that denote the boundaries between various regimes of filling behavior are strongly dependent upon the temperature. To confirm the accuracy of the theoretical results, we compare adsorption isotherms and density profiles calculated from nonlocal theory and Gibbs ensemble simulation. The results from theory and simulation are found to be in good agreement. We conclude with a discussion of the problems associated with estimating solid–fluid potential parameters from experiment for use in theoretical computations. A comparison of nonlocal theory model isotherms and experimental nitrogen uptake measurements on nonporous carbon is presented.

1. Introduction

Activated carbons and molecular sieve carbons are used in a variety of gas separation, purification, and reaction applications. Effective use of these materials requires knowledge of the sorbent structure and composition, that is, the pore geometry, pore size distribution, and functionality of the carbon surface. To this end, the nitrogen adsorption isotherm of the material offers a convenient means of characterization. The typical activated carbon is an interconnected network of graphitic pores, each with its own shape, width, and chemical heterogeneities. While we cannot hope to realistically model such a complicated structure in its entirety, we can reduce the problem to a more tractable yet meaningful form by assuming that (1) the carbon has a slit pore geometry, as originally proposed by Everett,[1] (2) the aspect ratio of pore length of pore width is large, so that pore junction effects can be neglected, and (3) the concentration of surface functional groups is low and can be disregarded. With these assumptions, the task of determining the pore size distribution $f(H)$ of the sorbent involves the solution of the adsorption integral

$$N(P) = \int_0^\infty dH \, f(H) \, \rho(P,H) \tag{1}$$

where $N(P)$ is the measured isotherm of the material, and $\rho(P,H)$ is the theoretical uptake of nitrogen in a slit pore of width H at pressure P. The shape of the overall isotherm $N(P)$ depends largely upon the size range of pores present in the carbon. IUPAC has designated a classification scheme for adsorption based upon the shape of the measured isotherm,[2] as well as a division of pores into several size groupings,[2,3] shown in Table I.

Historically, the solution of adsorption integrals such as eq 1 has employed macroscopic correlations or classical

† Cornell University.
‡ BP Research Centre.
⊕ Abstract published in *Advance ACS Abstracts*, August 15, 1993.
(1) Everett, D. H.; Powl, J. C. *J. Chem. Soc., Faraday Trans. 1* 1976, 72, 619.
(2) Sing, K. S. W.; Everett, D. H.; Haul, R. A. W.; Moscou, L.; Pierotti, R. A.; Rouquerol, J.; Siemieniewska, T. *Pure Appl. Chem.* 1985, 57, 603.
(3) Gregg, S. J.; Sing, K. S. W. *Adsorption, Surface Area and Porosity*; Academic Press: New York, 1982.

Table I. IUPAC Pore Size Classification Scheme[3]

type	pore size (Å)	type	pore size (Å)
macropore	≥500	supermicropore	7–20
mesopore	20–500	ultramicropore	≤7

thermodynamic models such as the Kelvin equation[4] to represent the local adsorption isotherm $\rho(P,H)$. However, modern statistical mechanical methods, namely, density functional theory and Monte Carlo molecularr simulation, provide a much more accurate context for interpreting isotherm data, particularly for microporous materials such as sieve carbons. Our objective in this paper is to investigate the theoretical adsorption of nitrogen in porous carbon using a density functional theory description of pore filling, in order to determine useful structural information for industrial carbons. In the next section, we develop a model for single pore adsorption based upon nonlocal density functional theory, and describe briefly the Gibbs ensemble simulation method. In section 3, we present and discuss theoretical isotherms generated from density functional theory and Gibbs simulation. The effects of pore size, temperature, and wall–fluid interaction strength are addressed. In section 4, we compare the model isotherms with experimental nitrogen adsorption measurements on a nonporous carbon sample. Finally, in section 5 we summarize our results and offer recommendations for additional improvements of the density functional theory model of adsorption in carbon.

2. Theory

2.1. Slit Pore Model. To model nitrogen adsorption on activated carbon, we select a slit pore geometry for the individual pores. The individual pore is represented as two semiinfinite parallel graphitic slabs separated by a physical width, H, the distance between the centers of the surface carbon atoms (Figure 1). The graphite layers in each slab are separated by a uniform spacing, Δ. By using infinite boundaries in the lateral directions, we implicitly

(4) Cranston, R. W.; Inkley, F. A. *Adv. Catal.* 1957, 9, 143.
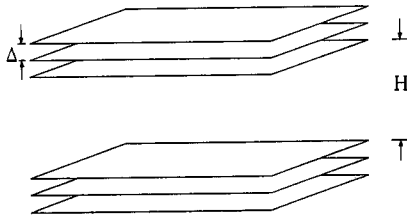
Figure 1. Carbon slit pore model.

Table II. Potential Parameters Used in Density Functional Theory and Gibbs Ensemble Simulations

param	value	param	value
Δ	3.35 Å	ϵ_{ff}/k	93.98 K
ρ_s	0.114 Å^{-3}	σ_{sf}	3.494 Å
σ_{ff}	3.572 Å	ϵ_{sf}/k	41.87, 49.03, 53.22 K

assume that the aspect ratio of pore length to pore width is large. Thus, we neglect the influence of connectivity in the pore model. We also assume that the graphite surface is uncorrugated, rigid, and chemically homogeneous.

For the fluid–fluid interaction potential ϕ_{ff}, we use the Lennard-Jones 12–6 pair potential

$$\phi_{ff}(r) = 4\epsilon_{ff}\left[\left(\frac{\sigma_{ff}}{r}\right)^{12} - \left(\frac{\sigma_{ff}}{r}\right)^6\right] \quad (2)$$

where r is the separation distance and ϵ_{ff} and σ_{ff} are fitted parameters for the bulk nitrogen well depth and molecular diameter. The solid–fluid interaction potential ϕ_{sf} for nitrogen interacting with a single graphitic slab is well described by the Steele 10–4–3 potential[5]

$$\phi_{sf}(z) = \epsilon_w\left[\frac{2}{5}\left(\frac{\sigma_{sf}}{z}\right)^{10} - \left(\frac{\sigma_{sf}}{z}\right)^4 - \frac{\sigma_{sf}^4}{3\Delta(z + 0.61\Delta)^3}\right] \quad (3)$$

where z is the distance from the graphite surface and σ_{sf} is the effective nitrogen–carbon intermolecular diameter. The wall potential parameter ϵ_w is given by

$$\epsilon_w = 2\pi\epsilon_{sf}\rho_s\sigma_{sf}^2\Delta \quad (4)$$

where ρ_s is the graphitic density and ϵ_{sf} is the Lennard-Jones well depth of the nitrogen–carbon atom site interaction. For a slit pore, the fluid molecule will interact with two graphite slabs; hence, the full external potential V_{ext} is written as

$$V_{ext}(z) = \phi_{sf}(z) + \phi_{sf}(H-z) \quad (5)$$

Table II summarizes the parameter values chosen for these potentials. The selection of these values is further discussed in section 4.

2.2. Density Functional Theory. Each individual slit pore has a fixed geometry, and is open and in contact with bulk nitrogen. The temperature is fixed at the nitrogen boiling point. For this system, the grand canonical ensemble provides the appropriate description of the thermodynamics. In this ensemble, the chemical potential μ, temperature T, and pore volume V are specified. In the presence of a spatially varying external potential V_{ext}, the grand potential functional Ω of the fluid is written as

$$\Omega[\rho_L(\mathbf{r})] = F[\rho_L(\mathbf{r})] - \int d\mathbf{r}\,\rho_L(\mathbf{r})[\mu - V_{ext}(\mathbf{r})] \quad (6)$$

where F is the intrinsic Helmholtz free energy functional, ρ_L is the local fluid density at position $\mathbf{r}$, and the integration is over the pore volume V. Expanding F perturbatively

about a reference system of hard spheres with diameter d, we obtain

$$F[\rho_L(\mathbf{r})] = F_h[\rho_L(\mathbf{r});d] + $$
$$(1/2)\int\int d\mathbf{r}\,d\mathbf{r}'\,\rho_L(\mathbf{r})\,\rho_L(\mathbf{r}')\,\phi_{att}(|\mathbf{r}-\mathbf{r}'|) \quad (7)$$

where F_h is the hard sphere Helmholtz free energy functional and ϕ_{att} is the attractive part of the fluid–fluid potential. In the second term on the right-hand side we have invoked the mean field approximation, wherein the correlations due to the attractive forces are neglected (i.e., the two-body distribution function $g(\mathbf{r})$ is set equal to unity). The attractive part of the fluid–fluid potential is represented by the Weeks–Chandler–Andersen formulation[6] of the Lennard-Jones potential

$$\phi_{att}(|\mathbf{r}-\mathbf{r}'|) = \phi_{ff}(|\mathbf{r}-\mathbf{r}'|), \quad |\mathbf{r}-\mathbf{r}'| > r_m$$
$$= -\epsilon_{ff}, \quad |\mathbf{r}-\mathbf{r}'| < r_m \quad (8)$$

where $r_m = 2^{1/6}\sigma_{ff}$ is the location of the minimum of the Lennard-Jones potential. The hard sphere term F_h is further split into an ideal gas component and an excess component

$$F_h[\rho_L(\mathbf{r}); d] = kT\int d\mathbf{r}\rho_L(\mathbf{r})[\ln(\Lambda^3\rho_L(\mathbf{r})) - 1] +$$
$$kT\int d\mathbf{r}\rho_L(\mathbf{r})\,f_{ex}[\bar{\rho}(\mathbf{r}); d] \quad (9)$$

where $\Lambda = h/(2\pi mkT)^{1/2}$ is the thermal deBroglie wavelength, m is the molecular mass of nitrogen, and h and k are the Planck and Boltzmann constants, respectively. The excess Helmholtz free energy per particle, f_{ex}, is calculated from the Carnahan–Starling hard sphere equation of state[7] using a smoothed density, defined as

$$\bar{\rho}(\mathbf{r}) = \int d\mathbf{r}'\,\rho_L(\mathbf{r}')\,w[|\mathbf{r}-\mathbf{r}'|;\bar{\rho}(\mathbf{r})] \quad (10)$$

The choice of the weighting function w depends on the version of density functional theory used. For highly inhomogeneous confined fluids, a smoothed or nonlocal density approximation is introduced, in which the weighting function is chosen to give a good description of the hard sphere direct pair correlation function for the uniform fluid over a wide range of densities. Several sets of weighting functions have been proposed to study fluids confined in pores.[8–10] In this work, we use Tarazona's model for the smoothing functions.[10] This model has been shown to give very good agreement with simulation results for the density profile and surface tension of hard sphere fluids near hard walls. The Tarazona prescription for the weighting functions uses a power series expansion in the smoothed density. Truncating the expansion at second order yields

$$w[|\mathbf{r}-\mathbf{r}'|;\bar{\rho}(\mathbf{r})] = w_0(|\mathbf{r}-\mathbf{r}'|) + w_1(|\mathbf{r}-\mathbf{r}'|)\,\bar{\rho}(\mathbf{r}) +$$
$$w_2(|\mathbf{r}-\mathbf{r}'|)\,\bar{\rho}(\mathbf{r})^2 \quad (11)$$

The expansion coefficients w_0, w_1, and w_2 are reported elsewhere.[10] The equivalent hard sphere diameter, d, is calculated as a function of temperature. The explicit form

(5) Steele, W. A. *Surf. Sci.* **1973**, *36*, 317. *The Interaction of Gases with Solid Surfaces*; Pergamon: Oxford, 1974.

(6) Weeks, J. D.; Chandler, D.; Andersen, H. C. *J. Chem. Phys.* **1971**, *54*, 5237.

(7) Reed, T. M.; Gubbins, K. E. *Applied Statistical Mechanics*; McGraw-Hill: New York, 1973. Carnahan, N. F.; Starling, K. E. *J. Chem. Phys.* **1969**, *51*, 635.

(8) Rosenfeld, Y. *Phys. Rev. Lett.* **1989**, *63*, 980.

(9) Kierlik, E.; Rosinberg, M. L. *Phys. Rev. A* **1990**, *42*, 3382.

(10) Tarazona, P. *Phys. Rev. A* **1985**, *31*, 2672; **1985**, *32*, 3148. Tarazona, P.; Marini Bettolo Marconi, U.; Evans, R. *Mol. Phys.* **1987**, *60*, 573.

approximates the Barker–Henderson diameter[11]

$$\frac{d}{\sigma_{ff}} = \frac{\eta_1 kT/\epsilon_{ff} + \eta_2}{\eta_3 kT/\epsilon_{ff} + \eta_4} \quad (12)$$

where the constants η_i are chosen to give good agreement between theory and simulation at low temperatures.[12] In this work we use $\eta_1 = 0.3837$, $\eta_2 = 1.035$, $\eta_3 = 0.4249$, and $\eta_4 = 1$. To solve for the equilibrium density profile, the grand potential functional is minimized with respect to the local density

$$\frac{\partial \Omega[\rho_L(\mathbf{r})]}{\partial \rho_L(\mathbf{r})}\bigg|_{\rho_L = \rho_{L,eq}} = 0 \quad (13)$$

For large pores, two minimum density profiles commonly arise. These are the liquid and vapor branches associated with thermodynamic hysteresis in individual slit pores. When more than one minimum exists, the density profile which has the lower grand potential energy is the stable branch. The chemical potential at which condensation occurs is the value for which the two minima have the same grand potential energy. For the model described in section 2.1, the density profile will be one dimensional; that is, the density varies in the z direction only. A numerical iteration scheme is used to solve the minimization condition for $\rho_L(z)$ over a range of chemical potentials μ for selected values of H. The chemical potential is related to the bulk reduced pressure P/P_0 through the bulk fluid equation of state. The mean pore fluid density ρ is calculated as

$$\rho = (1/H) \int_0^H \rho_L(z)\, dz \quad (14)$$

It is convenient to scale quantities with respect to the fluid–fluid parameters. In subsequent sections, we make reference to the following dimensionless quantities:

$$H^* = H/\sigma_{ff} \qquad T^* = kT/\epsilon_{ff}$$

$$\rho^* = \rho\sigma_{ff}^3 \qquad z^* = z/\sigma_{ff}$$

2.3. Gibbs Ensemble Monte Carlo.
To check the accuracy of the density functional theory results, we have performed adsorption calculations using the Gibbs ensemble simulation method. The full Gibbs methodology is described elsewhere;[13] here, we confine our description to a brief summary. The Gibbs ensemble provides a direct route to the determination of phase coexistence properties of fluids, by performing a simultaneous simulation in two distinct physical regions, generally having different densities, that are in thermal, mechanical, and material contact. Previously, Gibbs simulation has been used to determine phase equilibria in bulk fluids[13] and in fluids adsorbed in cylindrical pores.[14] Here, we carry out Gibbs ensemble calculations for fluid adsorption in the slit pore geometry of Figure 1.

Two types of Gibbs simulations are performed: pore–pore and pore–fluid. The pore–pore calculations yield the coexisting liquid and vapor densities at the filling pressures of the pores in which capillary condensation occurs. A schematic of the pore–pore simulation method is shown in Figure 2. The fluid molecules are confined within the slit pore geometry of the two simulation cells, which we designate regions I and II. At each simulation
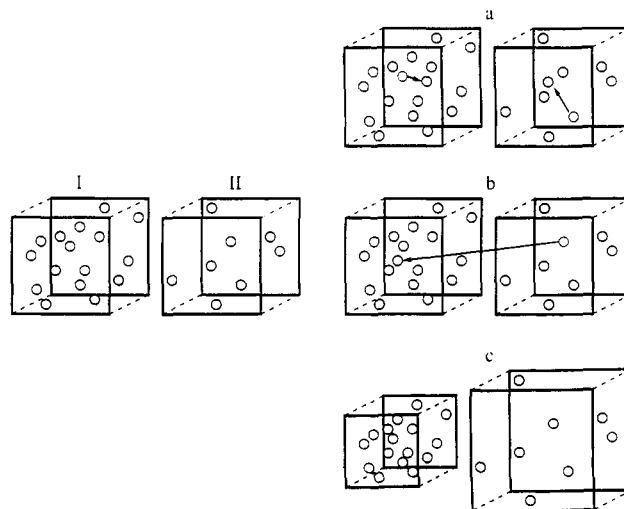

Figure 2. Gibbs ensemble Monte Carlo method for pore–pore equilibria calculations. The fluid in each region, I and II, is confined between two pore walls (denoted by the solid lines), separated by a fixed slit width. (Dashed lines delineate periodic boundaries.) From the sample configuration of regions I and II, three possible perturbations may be introduced: (a) displacement of molecules in each region, (b) interchange of molecules between regions I and II, and (c) exchange of pore surface area between regions I and II.

step, one of three perturbations is attempted: (a) particle displacements in each region; (b) particle interchange between the two regions; and (c) exchange of pore surface area between the two regions, such that the total surface area remains constant. The probability X that an attempted configuration will be accepted is

$$X = \min(1, \exp[-\Delta E/kT]) \quad (15)$$

where the change in total energy ΔE depends on the type of perturbation. For displacement steps,

$$\Delta E = \Delta E_I + \Delta E_{II} \quad (16)$$

where ΔE_i is the energy change in region i. (In practice, it is simpler to perform the displacement steps individually in each region, rather than to simultaneously attempt moves in each region. Statistically, the two procedures are equivalent and give the same calculated properties.) For particle interchange steps,

$$\Delta E = \Delta E_I + \Delta E_{II} + kT \ln \frac{(N_I + 1)V_{II}}{N_{II}V_I} \quad (17)$$

where N_i and V_i are the number of particles and volume, respectively, of region i. (Here $V_i = H\,A_i$, where A_i is the pore surface area of region i.) Finally, for exchange of surface area,

$$\Delta E = \Delta E_I + \Delta E_{II} - N_I kT \ln \frac{A_I - \Delta A}{A_I} - $$
$$N_{II} kT \ln \frac{A_{II} + \Delta A}{A_{II}} \quad (18)$$

where ΔA is the amount of surface area exchanged between the two regions. The sampling of configurations using these three perturbations ultimately brings the two regions into thermal, material, and mechanical equilibrium. Such a state is phase-equilibrated, and thus the Gibbs method yields the equilibrium densities of the coexisting liquid and vapor phases.

We use the potentials described in section 2.1 to model the fluid–fluid and fluid–solid interactions. Starting from an initial face-centered cubic lattice configuration in each

(11) Barker, J. A.; Henderson, D. *J. Chem. Phys.* **1967**, *47*, 4714.
(12) Telo da Gama, M. M. Unpublished data, 1985.
(13) Panagiotopoulos, A. Z. *Mol. Phys.* **1987**, *61*, 813.
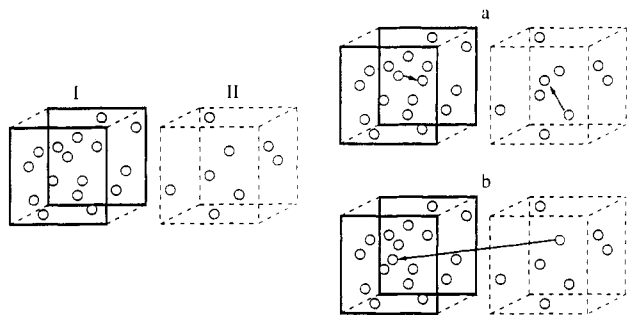(14) Panagiotopoulos, A. Z. *Mol. Phys.* **1987**, *62*, 701.

Figure 3. Gibbs ensemble Monte Carlo method for pore–fluid equilibria calculations. The fluid in region I is confined between two pore walls (denoted by the solid lines), separated by a fixed slit width. The fluid in region II is in the bulk state (the dashed lines delineate periodic boundaries). From the sample configuration of regions I and II, two possible perturbations may be introduced: (a) displacement of molecules in each region and (b) interchange of molecules between regions I and II.

region, the system is equilibrated by successive perturbations over a sufficient number of configurations. Additional configurations are then sampled to measure the properties of the equilibrated phases. Displacements, particle interchanges, and volume exchanges are performed in the ratio $N:f_I:1$, where N is the total number of particles in the two regions (typically 512–1000) and f_I is an adjustable interchange parameter. Because the probability of successful particle interchange decreases exponentially with decreasing temperature, a sufficiently large value of f_I (usually 400–500) is selected to ensure adequate material interchange between the two regions. A typical calculation requires approximately 1.5 million configurations for equilibration and an additional 1.5 million configurations for collecting property data.

For the inhomogeneous confined fluid, long-range corrections are not computed because of the associated computational difficulties. However, the system size is chosen so that the minimum edge length of the pore surface is $10\sigma_{ff}$ (i.e., all molecular interactions up to a distance of $5\sigma_{ff}$ are explicitly included in the calculations). This cutoff is presumed to be large enough so that long-range corrections may be neglected.

While the pore–pore calculation yields the equilibrium vapor and liquid states that coexist in a pore of specified width, it does not specify the pressure at which the equilibrium state occurs, nor does it indicate the amount adsorbed at pressures below and above the equilibrium pressure. To determine the filling pressure, and the state points along the vapor and liquid branches of the adsorption isotherm, we use the Gibbs pore–fluid ensemble. A schematic of the pore–fluid calculation is shown in Figure 3. In this version of Gibbs simulation, the fluid in region I is again confined in a slit pore, but the fluid in region II is in the bulk state (all boundaries are periodic). In the pore–fluid calculation, there are no attempted exchanges of volume, as the condition for mechanical equilibrium is automatically satisfied if the chemical potentials in regions I and II are equal (i.e., material equilibrium).[15] Hence, only displacement and particle interchange steps are performed, with the same acceptance probabilities as stated for the aforementioned pore–pore calculation. We follow Panagiotopoulos[13] and include long-range corrections for a cubic simulation cell geometry in the bulk property calculations.[16] At equilibrium, we obtain the adsorbed fluid density corresponding to the bulk fluid pressure. To aid comparison with theory and experiment,
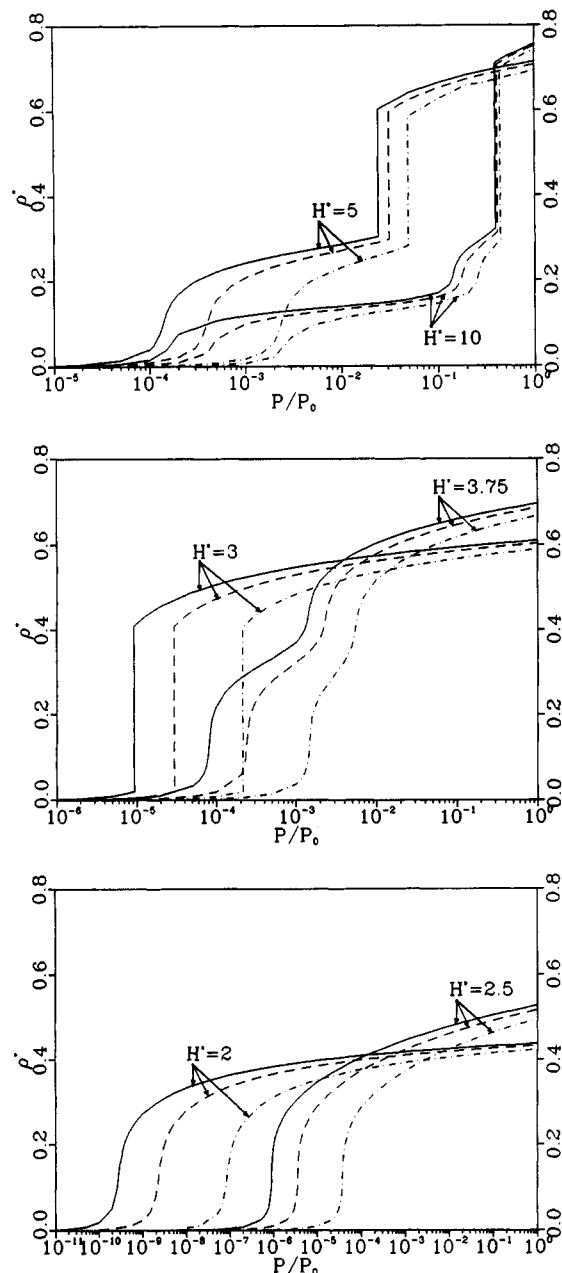

Figure 4. Adsorption as a function of solid–fluid potential strength for nitrogen uptake in carbon slit pores at 77 K: (a, top) $H^* = 10$ and 5, (b, middle) $H^* = 3.75$ and 3, (c, bottom) $H^* = 2.5$ and 2. The lines show the nonlocal theory isotherms for $\epsilon_{sf}/k = 53.22$ K (solid lines), 49.03 K (dashed lines), and 41.87 K (dotted–dashed lines).

we scale the pressure with respect to the saturation pressure P_0 of the bulk Lennard-Jones fluid, given by the modified Benedict–Webb–Rubin equation of state.[17] To determine the pressure at which condensation occurs, we interpolate the vapor coexistence density from the pore–pore calculation so that it coincides with the vapor branch of the isotherm constructed from the pore–fluid results.

3. Results

3.1. Effect of the Wall Potential. We first examine the influence of the solid–fluid potential strength ϵ_{sf} on the adsorption isotherm. In Figure 4, the nonlocal theory results for the nitrogen isotherm on carbon at $T = 77$ K are shown for three values of ϵ_{sf} and several slit widths. In

(15) Henderson, J. R. *Mol. Phys.* **1983**, *48*, 715.
(16) Theodorou, D. N.; Suter, U. W. *J. Chem. Phys.* **1985**, *82*, 955.

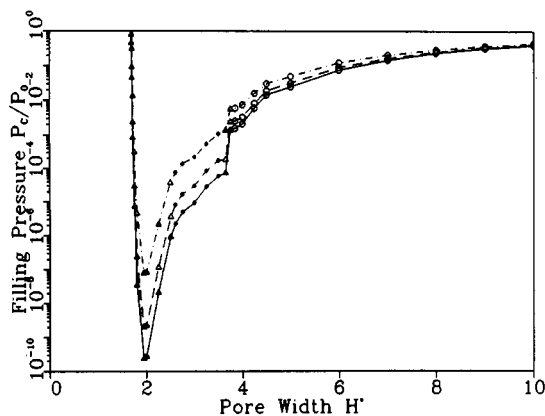(17) Johnson, J. K.; Zollweg, J. A.; Gubbins, K. E. *Mol. Phys.* **1993**, *78*, 591.

Figure 5. Filling pressures predicted by nonlocal theory for nitrogen in a carbon slit pore at 77 K. The lines show the filling pressures for ϵ/k = 53.22 K (solid lines), 49.03 K (dashed lines), and 41.87 K (dotted–dashed lines). The symbols denote the type of filling behavior: capillary condensation (open circles), monolayer transition (filled circles), and continuous filling (triangles).

all cases, increasing the solid–fluid well depth decreases the filling pressure. For mesopores (Figure 4a) the variations in the condensation pressure are slight, although the pressure at which the monolayer forms is, as one might anticipate, strongly dependent on ϵ_{sf}. For micropores (Figure 4b,c) the value of ϵ_{sf} has a strong influence on the pore filling pressure. For example, raising the solid–fluid potential strength from ϵ_{sf}/k = 41.87 K to ϵ_{sf}/k = 53.22 K (an increase of 27%) decreases the filling pressure of the ultramicropore H^* = 2 by almost 3 orders of magnitude. This has important implications regarding the accuracy of pore size distribution analysis, discussed in section 4.

We further observe that although the filling pressure strongly depends upon the solid–fluid potential strength, the shape of the isotherm for a given slit width is not similarly influenced by the solid–fluid potential parameter. Although the types of filling vary widely among the pore widths selected in Figure 4, for fixed H the filling behavior is the same for all the values of ϵ_{sf} considered. This occurs because for this range of ϵ_{sf} the wall–fluid potential strength ϵ_w is about ten times greater than the fluid–fluid potential strength. Only at much smaller values of the solid–fluid potential, where ϵ_w approaches ϵ_{ff}, would changes in the type of filling be observed.[18]

Figure 5 summarizes the effect of the solid–fluid potential interaction on the filling pressure over a range of pore widths. For pores which fill continuously (e.g., H^* = 3.75, 2.5, 2) the filling pressure is estimated from the inflection point of the isotherm. Clearly, the variation in the filling pressure becomes most pronounced in the micropore band (H^* < 4). The location of the minimum in the filling pressure, at approximately H^* = 2, provides a benchmark for the range of pressures that must be sampled to completely characterize all pore widths in a sorbent with a distribution of pore sizes (e.g., activated carbon).

3.2. Adsorption and the Slit Width. Individual pore isotherms were generated using nonlocal theory for a range of pore sizes from H^* = 1.68 to H^* = 100 (6.0–357 Å) at T = 77 K for each of the three values of the solid–fluid potential well depth introduced in section 3.1. In the remainder of section 3, we confine our attention to the set of isotherms corresponding to ϵ_{sf}/k = 53.22 K.

The nitrogen adsorption isotherms in carbon mesopores are shown in Figure 6. Pores in this size range exhibit
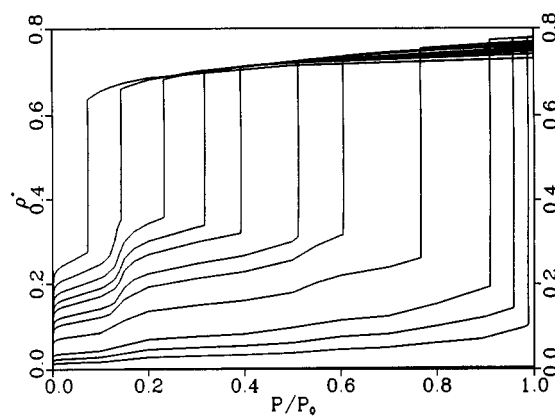
(18) Balbuena, P. B.; Gubbins, K. E. *Fluid Phase Equilib.* **1992**, *76*, 21. Balbuena, P. B.; Gubbins, K. E. *Langmuir*, in press.

Figure 6. Nonlocal theory isotherms for nitrogen adsorbed in mesoporous carbon slits at 77 K. The pore widths, reading from left to right, are H^* = 6, 7, 8, 9, 10, 12, 14, 20, 40, 60, and 100. The line at the bottom of the figure shows the bulk vapor density.
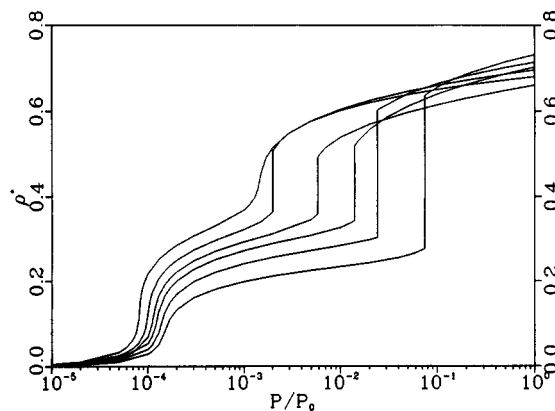

Figure 7. Low-pressure nitrogen condensation range of the smaller mesoporous slit carbons, calculated from nonlocal theory at 77 K. Reading from left to right, the pore widths are H^* = 3.75, 4, 4.25, 4.5, 5, and 6.

capillary condensation, or type IV behavior in the IUPAC classification scheme. At low pressures, the monolayer is formed; as the pressure is increased, additional multilayers are adsorbed, until the condensation pressure is reached, whereupon a phase transition to the liquid state occurs. Above the condensation pressure, there is a gradual increase in the mean density due to the compression of the nitrogen in the liquid-filled pore.

As the pore width is reduced, the condensation pressure decreases (see Figure 7). This is explained by considering the solid–fluid slit potentials, shown for several pore widths in Figure 8. As the slit walls move closer together, the bulklike region in the center of the pore (e.g., Figure 8a), where V_{ext} is approximately zero, disappears, and adsorption is enhanced throughout the pore space (Figure 8b,c). Additionally, the proximity of adsorbed fluid layers on opposing walls increases fluid–fluid interactions, thus further promoting the adsorption of multilayers. A transition from capillary condensation to continuous filling occurs at a critical width of H_{c1}^* = 3.8, or 13.6 Å (note isotherm H^* = 3.75 in Figure 7).

Interestingly, there is a second region of discontinuous pore filling in the nonlocal theory isotherms, separate from the condensation region, at pore widths below the critical width H_{c1}^*. Figure 9 shows that, for the range of pore widths between H_{c3}^* = 2.55 (9.1 Å) and H_{c2}^* = 3.6 (12.8 Å), a 0 → 1 monolayer transition occurs wherein the incomplete monolayer on each pore wall abruptly fills to completion. A narrow band of continuously filling pores is found between H_{c2}^* and H_{c1}^*. Although the pores in the
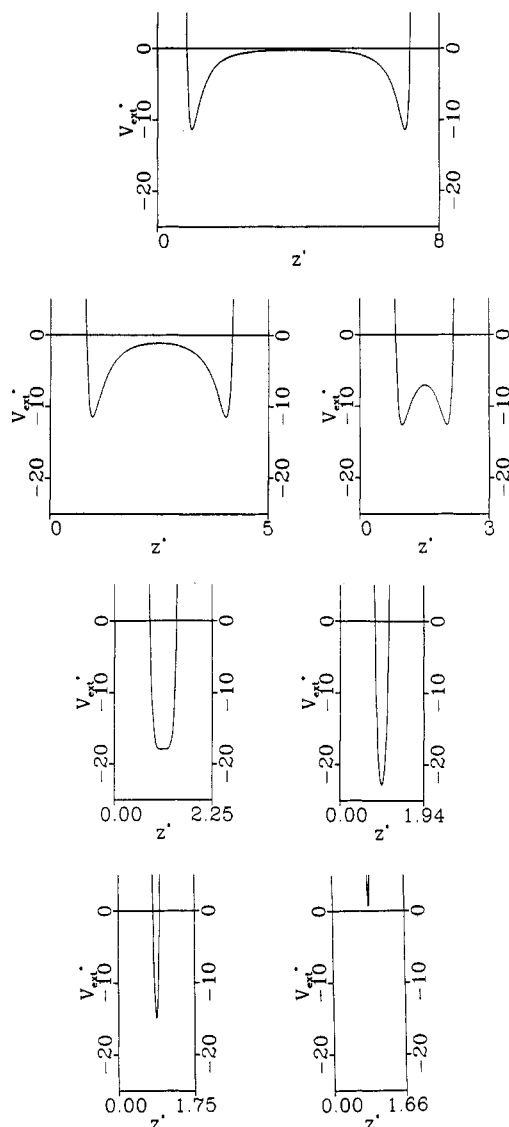
Figure 8. Solid–fluid potentials $V^*_{ext} = V_{ext}/\epsilon_{ff}$ for nitrogen in carbon slits: (a, top) $H^* = 8$, (b, second row, left) $H^* = 5$, (c, second row, right) $H^* = 3$, (d, third row, left) $H^* = 2.25$, (e, third row, right) $H^* = 1.94$, (f, bottom, left) $H^* = 1.75$, (g, bottom, right) $H^* = 1.66$.
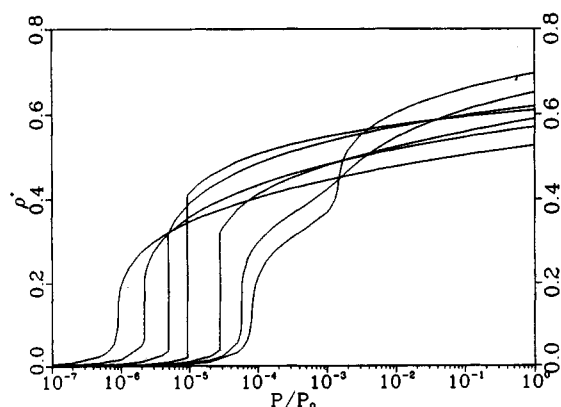

Figure 9. Monolayer transitions in the nonlocal theory isotherms of nitrogen in carbon supermicropores at $T = 77$ K ($T^* = 0.823$). Reading from left to right, $H^* = 2.5$, 2.6, 2.75, 3, 3.25, 3.5, and 3.75.

size range from H^*_{c3} to H^*_{c2} fall within the IUPAC supermicropore classification (Table I), the phase transition in these slits is atypical of the continuous filling normally expected in such pores. However, Gibbs en-
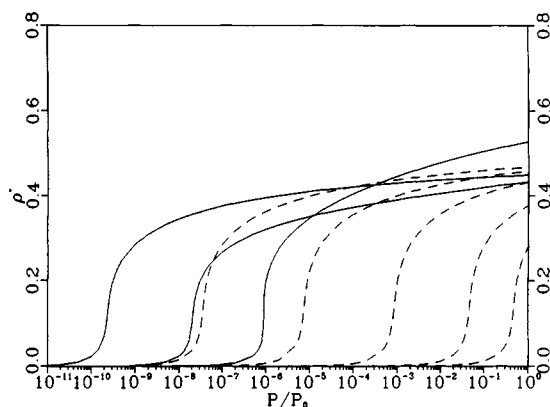

Figure 10. Nonlocal theory isotherms for nitrogen in carbon ultramicropores at 77 K. The solid isotherms, reading from left to right, are $H^* = 1.94$, 2.25, and 2.5. For pore widths below $H^* = 1.94$, the filling pressure *increases* with decreasing width, as shown by the set of dashed isotherms (reading from left to right): $H^* = 1.8$, 1.75, 1.72, 1.7, and 1.69.

semble Monte Carlo simulations (section 3.3) confirm the presence of the $0 \rightarrow 1$ monolayer transition in pores that can accommodate approximately two complete layers of molecules.

For still smaller pore widths, we observe a return to continuous filling (Figure 10). Pores in this size range, which corresponds to the IUPAC ultramicropores, are too narrow to accommodate more than a single layer of molecules. The shapes of the ultramicropore isotherms are similar to that of the IUPAC type I isotherm, characteristic of micropore adsorption, although the IUPAC representation uses a linear rather than a logarithmic pressure axis.

As Figure 8d indicates, the two minima of the solid–fluid potential coalesce into a single minimum at a pore width of $H^* = 2.25$ (8.0 Å). This results in an enhancement of the potential well strength, which is maximized to roughly double its original depth at a pore width of $H^* = 1.94$, or 6.9 Å (Figure 8e). A corresponding reduction in the filling pressure is seen, with the minimum (at $H^* = 1.94$) occurring at approximately $P/P_0 = 10^{-10}$, a pressure on the order of 0.1 μTorr. As the pore width is reduced beyond this minimum, the repulsive parts of the opposing wall potentials begin to overlap (Figure 8f), until the entire solid–fluid slit potential becomes repulsive (Figure 8g). Hence, there is a rapid rise in filling pressure as the pore width drops below $H^* = 1.94$ (dashed lines in Figure 10). For pores with physical width narrower than $H^* = 1.69$ (6.0 Å), the pore space is inaccessible to nitrogen and no adsorption occurs. We note, finally, that the mean density of nitrogen in the ultramicropores is considerably reduced due to exclusion of the fluid molecules from the region near the slit walls. Only in the largest mesopores (see Figure 6) does the mean density in the pore approach the bulk saturated liquid value of $\rho^* = 0.792$.

While the IUPAC designation of pore sizes (Table I) is a useful guide to anticipating filling behavior, it is evident from the results presented here that the type of adsorption depends as much upon the adsorbate characteristics as it does upon the structure of the adsorbent. For example, if the size of the adsorbate molecule was increased, some of the slits that exhibited capillary condensation for the original value of σ_{ff} would fill continuously for the larger adsorbate diameter. Therefore, it is more relevant to devise a classification scheme that uses a pore size scaled with respect to the adsorbate diameter, and that also accounts for the influence of temperature. We shall return to the latter point in section 3.4.
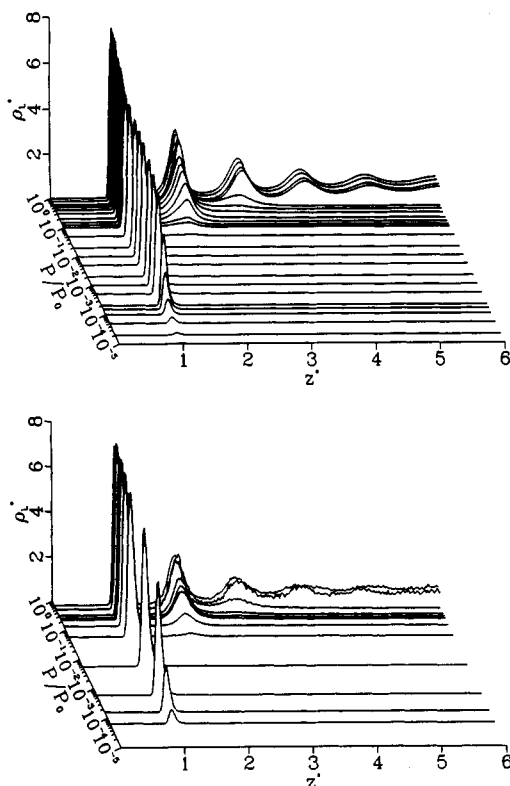
Figure 11. Local density profiles for nitrogen adsorption at 77 K in a slit pore of width $H^* = 12$: (a, top) nonlocal theory, (b, bottom) Gibbs ensemble Monte Carlo. The horizontal axis denotes distance from the center of the carbon atoms of the graphite surface. (The profile is symmetric about the center line of the slit at $z^* = 6$.) The local fluid density (vertical axis) is plotted for a sequence of reduced pressures (axis into the page).

Figure 12. Local density profiles for nitrogen adsorption at 77 K in a slit pore of width $H^* = 3$: (a, top) nonlocal theory, (b, bottom) Gibbs ensemble Monte Carlo. The horizontal axis denotes distance from the center of the carbon atoms of the graphite surface. (The profile is symmetric about the center line of the slit at $z^* = 1.5$.) The local fluid density (vertical axis) is plotted for a sequence of reduced pressures (axis into the page).

3.3. Comparison of Nonlocal Theory and Gibbs Simulation.

In Figure 11, we compare the filling behavior of the mesoporous carbon slit of width $H^* = 12$ predicted by nonlocal theory and Gibbs ensemble Monte Carlo. The local density profile of nitrogen in the slit is shown in Figure 11a for the nonlocal theory calculation. In this figure the local density is plotted as a function of increasing pressure at fixed temperature $T = 77$ K and solid–fluid potential $\epsilon_{sf}/k = 53.22$ K. At this potential strength, a monolayer forms at $P/P_0 = 10^{-4}$. As the pressure increases, a second and third multilayer form, until the filling pressure of $P_C/P_0 = 0.512$ is attained. At this point, condensation occurs, and thereafter the entire pore is liquid-filled, as the oscillatory density profile at high pressure indicates. In Figure 11b, the corresponding density profiles computed from Gibbs ensemble calculations are shown. The similarity between the two plots demonstrates the ability of nonlocal theory to describe filling in the highly inhomogeneous pore environment.

A similar comparison of theoretical and simulation density profiles is presented in Figure 12 for the micropore $H^* = 3$. The nonlocal theory and Gibbs simulation profiles are again observed to be consistent, demonstrating the applicability of the theory to modeling both mesopore and micropore filling. The Gibbs result also verifies the presence of the $0 \rightarrow 1$ monolayer transition found in the theoretical isotherms for supermicropore-sized slits.

Adsorption isotherms calculated from theory and simulation are compared in Figure 13, for the pore widths $H^* = 12, 5, 3,$ and 2.5. In each case, the filling pressures predicted by nonlocal theory and Gibbs simulation are in excellent agreement. Furthermore, the vapor and liquid branches of the theoretical and simulation isotherms agree quantitatively over the range of pressures sampled. There
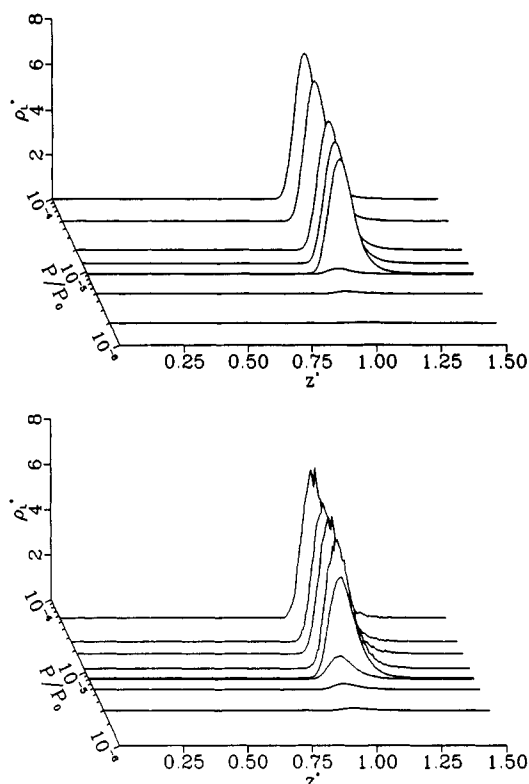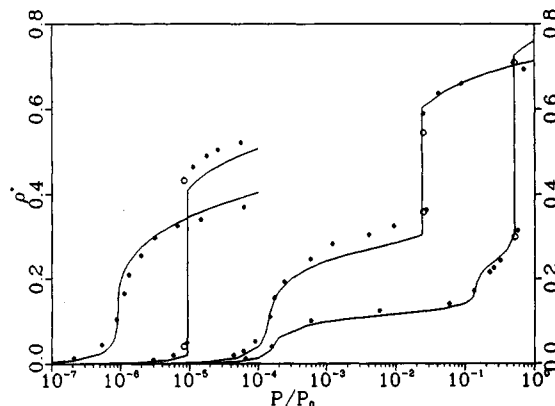

Figure 13. Comparison of nitrogen adsorption isotherms calculated from nonlocal theory and Gibbs ensemble simulation, for adsorption in carbon slits at 77 K. Lines denote the nonlocal theory results for pores of width (reading from left to right) $H^* = 2.5, 3, 5,$ and 12. Symbols show the corresponding Gibbs ensemble Monte Carlo calculations for these slit widths. Open circles indicate equilibrium densities from pore–pore calculations; solid circles show the results of pore–fluid calculations.

are some differences between theory and simulation for the adsorbed densities in smaller pores; this may arise because mean-field density functional theory predicts a higher bulk fluid critical temperature T_c than is obtained from simulations of the Lennard-Jones fluid.[19] Hence, the nonlocal theory isotherms at $T = 77$ K are at a lower reduced temperature T/T_c than the corresponding Gibbs simulation isotherms, and as a result the phase splitting in the theoretical calculation is more pronounced than in

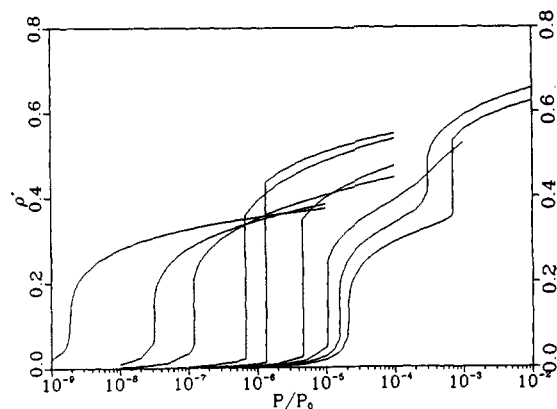(19) Lu, B. Q.; Evans, R.; Telo da Gama, M. M. *Mol. Phys.* **1985**, *55*, 1319.

Figure 14. Nonlocal theory isotherms of nitrogen adsorption in carbon supermicropores at $T = 70$ K ($T^* = 0.75$). Reading from left to right, $H^* = 2.25$, 2.4, 2.5, 2.75, 3, 3.25, 3.5, 3.75, and 4.1.
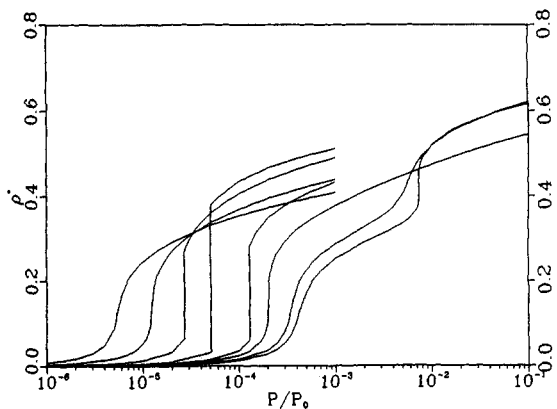

Figure 15. Nonlocal theory isotherms of nitrogen adsorption in carbon supermicropores at $T = 85$ K ($T^* = 0.9$). Reading from left to right, $H^* = 2.5$, 2.6, 2.75, 3, 3.25, 3.4, 3.75, and 4.

the Gibbs simulation. Overall, however, the nonlocal theory provides a quantitatively accurate description of pore filling.

3.4. Effect of Temperature. Finally, we examine the variation of the adsorption isotherm with temperature at a fixed value of the solid–fluid potential strength. In Figures 14 and 15, the nitrogen isotherms of the supermicropores are shown for $\epsilon_{sf}/k = 53.22$ K at $T = 70$ and 85 K, respectively. These two temperatures bracket the previous calculation for the supermicropores at 77 K, shown in Figure 9. It is seen that the critical slit widths H_{c1}, H_{c2}, and H_{c3} at which the filling transitions occur depend upon the temperature. At the nitrogen boiling point of $T = 77$ K (Figure 9), we find that $H_{c1} > H_{c2}$, and hence there is a continuous filling band of supermicropores, as described in section 3.2. At the higher (but still subcritical) temperature of Figure 15, the difference between H_{c1} and H_{c2} increases and the range of continuous filling pores is broadened. At the lower temperature of 70 K (Figure 14), however, the critical slit width for layering exceeds the critical width for capillary condensation ($H_{c1} < H_{c2}$). At this temperature, there are no continuously filling pores, but instead a set of pore widths which exhibit two discontinuous jumps in the isotherm (e.g., the isotherm for $H^* = 3.75$ in Figure 14). These "stepped" or IUPAC type VI isotherms have been observed for the low-temperature adsorption of simple gases on carbon surfaces,[3] such as krypton on carbon black at 90 K.

The influence of temperature on the filling behavior is summarized in Figure 16, where the type of isotherm predicted by nonlocal theory is classified as a function of reduced temperature and reduced pore width. The lines
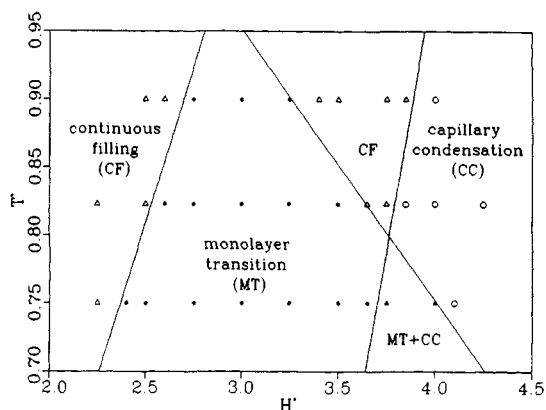

Figure 16. Coexistence diagram for nitrogen adsorption in carbon micropores. The filling behavior is plotted as a function of slit width for three temperatures. The symbols denote the type of filling observed: capillary condensation (open circles), monolayer transition (filled circles), continuous filling (open triangles), and the stepped isotherm (filled triangles), a combination of layering and condensation. The lines demarcate approximate boundaries between the various regimes of filling behavior.

approximate the boundaries between the various filling regimes and correspond to the temperature-dependent critical widths $H_{c1}(T)$, $H_{c2}(T)$, and $H_{c3}(T)$. It is evident from inspection of Figure 16 that the $0 \rightarrow 1$ monolayer phase transition is principally a low-temperature phenomenon; extrapolation of the critical lines in Figure 16 suggests that an upper critical temperature for the monolayer transition in nitrogen adsorption should occur slightly below $T^*_{cm} = 1.0$ (94 K). This critical temperature lies intermediate between the bulk Lennard-Jones fluid two-dimensional[20] and three-dimensional[21] critical temperatures of $T^*_{2D} = 0.515$ and $T^*_{3D} = 1.316$, respectively. The pores which exhibit the $0 \rightarrow 1$ monolayer transition condense two layers of molecules, one on each surface. Thus, it follows that $T_{cm} < T_{3D}$, due to the effect of confinement, and $T_{cm} > T_{2D}$, since the adsorbed molecules interact with molecules in the opposing film layer as well as in their own layer, and hence the fluid is not strictly two-dimensional. Clearly, the mapping in Figure 16 underscores the importance of including the effect of temperature in any comprehensive classification scheme for pore filling.

4. Discussion

The results presented in section 3 constitute a useful parametric characterization of adsorption in the carbon slit pore. However, in order to apply the predictions of nonlocal theory to the modeling of experimental data, it is necessary to relate the sorbent and fluid parameters as realistically as possible to experimental measurements. To this end, the nitrogen fluid–fluid parameters ϵ_{ff} and σ_{ff} are readily fitted so as to reproduce the bulk nitrogen saturated liquid density of 0.028 87 mol cm^{-3} and saturation pressure of 1 atm at the normal nitrogen boiling point of 77.347 K.[22] Similarly, the graphite interlayer spacing Δ and graphitic density ρ_s are well-established from previous investigations.[5]

Estimation of the solid–fluid parameters ϵ_{sf} and σ_{sf} is more problematic, as these values must be fitted to some representative measure of the adsorption interface. For

(20) Smit, B.; Frenkel, D. *J. Chem. Phys.* **1991**, *94*, 5663.
(21) Smit, B. *J. Chem. Phys.* **1992**, *96*, 8639.
(22) *CRC Handbook of Chemistry and Physics*, 61st ed.; Weast, R., Ed.; CRC Press: West Palm Beach, FL, 1981.
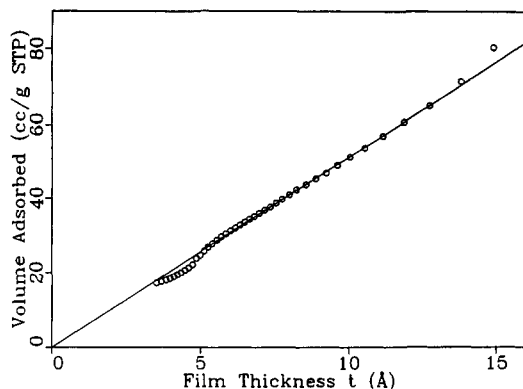
Figure 17. Surface area measurement of Vulcan nonporous carbon using the method of deBoer et al.[24] The slope of the linear region of the fit is the specific surface area of the sorbent.

the important problem of determining the pore size distribution of a mesoporous or microporous carbon, a sensible strategy is to fit the solid–fluid interaction parameters such that the theoretical model reproduces the nitrogen adsorption isotherm on a nonporous carbon surface. The theoretical adsorption isotherm is relatively insensitive to variations in σ_{sf}; hence, we use the Lorentz–Berthelot mixing rule (arithmetic mean) to evaluate the solid–fluid molecular diameter. To fit the solid–fluid well depth parameter, we might consider using a nonporous graphitic carbon such as Vulcan as a reference. In a sufficiently large slit pore, the adsorption on either surface can be taken as independent of the wetting on the other surface (see Figure 8a). Hence, a large mesopore (e.g., H^* = 100) can serve as an effective nonporous surface for estimating ϵ_{sf}. The theoretical adsorption of nitrogen in a large mesopore can be converted to an equivalent uptake of nitrogen on a nonporous substrate by the equation

$$V_{ads} = (1/2)\rho_{NLT} H S V_{STP} \qquad (19)$$

where V_{ads} is the uptake of nitrogen (cm³ at STP/g of carbon), ρ_{NLT} is the mean density of nitrogen in the mesopore, H is the mesopore width, S is the surface area of adsorbed film per gram of carbon, and V_{STP} is the molar volume of nitrogen at standard conditions. The factor of 1/2 appears in the above equation since the mean density of nitrogen in the pore includes the wetting on both surfaces. Using experimental uptake data for V_{ads}, the solid–fluid potential parameter ϵ_{sf} can be fitted by finding the value which gives a nonlocal theory isotherm ρ_{NLT} satisfying the above equation. To use this equation, we need an accurate estimate of S, the specific surface area of the adsorbed film. This value could be taken as the BET surface area of the carbon; however, experimental evidence suggests that the actual surface area of nonporous carbon is 10% greater than the area computed from nitrogen BET measurements.[23] We follow the method of deBoer et al.[24] and estimate S from the slope of the plot of volumetric uptake against the universal film thickness, or "t curve", of nitrogen on carbon. The result for nitrogen adsorption on nonporous Vulcan at 77 K is shown in Figure 17; the surface area is calculated from the slope S_{lin} of the linear region as

$$S = S_{lin}/(\rho_{ads} V_{STP}) \qquad (20)$$

where ρ_{ads} is the density of the adsorbed film. Here we take ρ_{ads} to be equal to the bulk saturated liquid nitrogen
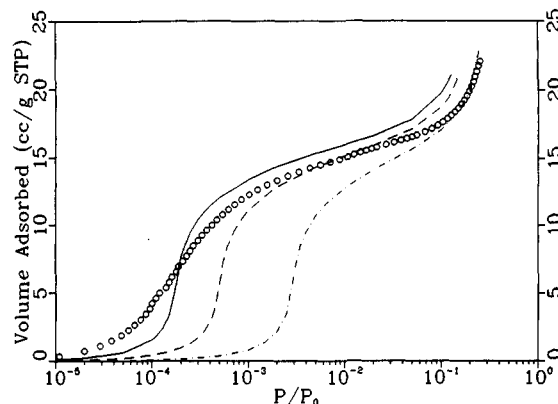

Figure 18. Comparison of theoretical and experimental isotherms for nitrogen on nonporous carbon at 77 K. The symbols show the Vulcan isotherm measured by experiment. The lines display the isotherms predicted by nonlocal theory for ϵ_{sf}/k = 53.22 K (solid line), 49.03 K (dashed line), and 41.87 K (dotted-dashed line).

density, though it is possible that the film actually has a more solidlike density. We obtain S = 78.6 m²/g, compared to 71.76 m²/g from BET measurement. The ratio S/S_{BET} = 1.10 is consistent with deBoer's results for Graphon and Spheron carbon blacks.[23]

Using this specific surface area, the nonlocal theory results are fitted to the experimental Vulcan uptake data as shown in Figure 18. Clearly the pressure at which the monolayer forms is very sensitive to the value of ϵ_{sf}; for Vulcan, the best fit is obtained at ϵ_{sf}/k = 53.22 K. The isotherm at ϵ_{sf}/k = 49.03 K overlaps well in the pressure range from $P/P_0 = 10^{-3}$ to $P/P_0 = 10^{-1}$, while the higher pressure region corresponding to the second adsorbed layer seems to be best fit by the ϵ_{sf}/k = 41.87 K isotherm. In this circumstance, one must choose the portion of the isotherm that is most representative of the solid–fluid interactions. In general, the low-pressure (monolayer) regime can be given priority since the low adsorbed density at these pressures minimizes the fluid–fluid forces. The set of model isotherms at ϵ_{sf}/k = 53.22 K was recently used successfully to determine the pore size distributions of several microporous activated carbons from nitrogen adsorption measurements.[25]

Since the solid–fluid potential strength was demonstrated to strongly influence the filling pressures of micropores, it is essential that this parameter is carefully fitted for applications involving pore size distribution analysis. The present fitting method requires estimation of the adsorbed film density, a quantity that is not readily known. Also, the imperfectness of the fit suggests that other factors need to be accounted for, such as the nitrogen quadrupole, the nonspherical shape of the nitrogen molecule, and the difference in the reduced temperatures of mean-field theory and simulation (section 3.3). Nonetheless, the nonlocal theory model provides a practical guide to the wall–fluid interaction parameter. Other methods, e.g., using isosteric heat of adsorption data, may provide an alternative, and perhaps less ambiguous, route to estimating the model parameters.

5. Conclusion

The nonlocal theory model of adsorption in a carbon slit pore has been found to predict adsorption isotherms and phase transitions that are in excellent agreement with

(23) de Boer, J. H.; Linsen, B. G.; Osinga, T. J. *J. Catal.* **1965**, *4*, 643.
(24) Lippens, B. C.; Linsen, B. G.; de Boer, J. H. *J. Catal.* **1964**, *3*, 32.

(25) Lastoskie, C. M.; Gubbins, K. E.; Quirke, N. *J. Phys. Chem.* **1993**, *97*, 4786.

Gibbs ensemble Monte Carlo results. The effects of pore size, temperature, and the strength of the solid–fluid potential interactions have been examined. It is observed that, for the range of solid–fluid potential strengths representative of many graphitic carbons, increasing the interaction strength markedly decreases the filling pressures of slit pores, especially for microporous slits. The potential strength does not seem to affect the type of filling observed, however. Several regimes of pore filling were observed, depending in part upon the size of the slit pore. In addition to the usual transition from condensation to continuous filling at some critical mesopore width, a layering transition in the monolayer is observed in some supermicropores. The critical widths at which transitions between these types of filling occur are strongly dependent on the temperature. Low temperatures give rise to steplike isotherms in the supermicropores, whereas higher (though still subcritical) temperatures yield a broader range of continuously filling supermicropores.

The nonlocal theory model was also demonstrated to provide a satisfactory fit to experimental uptake measurements of nitrogen on nonporous carbon. Hence, the model can be used to predict pore size distribution information.[25] A drawback of the present model is that it does not incorporate orientational effects of the nitrogen molecule. Also, the discrepancy in the bulk critical temperatures predicted by nonlocal theory and simulation is likely to cause some differences in the curvature of the isotherms predicted by the two methods. Our future work will address these issues.